Application of fractal models to delineate mineralized zones in the Pulang porphyry copper deposit, Yunnan, Southwest China

Xiaochen Wang[a], Qinglin Xia[a,b,*], Tongfei Li[a], Shuai Leng[a], Yanling Li[a], Li Kang[a], Zhijun Chen[a], Lianrong Wu[c]

[a] Faculty of Earth Resources, China University of Geosciences, Wuhan 430074, China

[b]Collaborative Innovation Center for Exploration of Strategic Mineral Resources, Wuhan 430074, China

[c]Yunnan Diqing Nonferrous Metal Co., Ltd., Shangri-La 674400, China

Abstract

The aim of this study is to delineate and identify various mineralized zones and barren host rocks based on surface and subsurface lithogeochemical data from the Pulang porphyry copper deposit, Southwest China, utilizing the number-size (N-S), concentration-volume (C-V) and power spectrum-volume (S-V) fractal models. The N-S model reveals three mineralized zones characterized by Cu thresholds of 0.28% and 1.45%: <0.28% Cu represents weakly mineralized zones and barren host rocks, 0.28%-1.45% Cu represents moderately mineralized zones, and >1.45% Cu represents highly mineralized zones. The results obtained by the C-V model depict four geochemical zones defined by Cu thresholds of 0.25%, 1.48% and 1.88%, representing nonmineralized wall rocks (Cu<0.25%), weakly mineralized zones (0.25%-1.48%), moderately mineralized zones (1.48%-1.88%), and highly mineralized zones (Cu>1.88%). The S-V model is used by performing a 3D fast Fourier transformation of assay data in the frequency domain. The S-V model reveals three mineralized zones characterized by Cu thresholds of 0.23% and 1.33%: <0.23% Cu represents leached zones and barren host rocks, 0.23%-1.33% Cu represents hypogene zones, and >1.33% Cu represents supergene enrichment zones. All the multifractal models indicate that high-grade mineralization occurs in the central and southern parts of the ore deposit. Their results are compared with the alteration and mineralogical models resulting from the 3D geological model using a logratio matrix. The results show that the S-V model is best at identifying highly mineralized zones in the deposit. However, the results of the C-V model for moderately and weakly mineralized zones are more accurate than those obtained from the N-S and S-V models.

Keywords: Fractal; Concentration-volume (C-V) model; Number-size (N-S) model; Power spectrum-volume (S-V) model; Mineralized zone; the Pulang porphyry copper deposit

1. Introduction

The definition and delineation of different mineralized zones and non–mineralized wall rocks are the main goal in economic geology and mineral exploration. Investigation of ore mineralogy and paragenetic sequence provides useful data on ore-forming processes in deposits because typical characteristics of various types of ore deposits are reflected by their mineral assemblages (Craig and Vaughan, 1994; White and Hedenquist, 1995). Common methods generally use mineralography, petrography and alteration mineral assemblage analysis to delineate various mineralized zones in porphyry deposits (Beane, 1982; Schwartz, 1947; Sillitoe, 1997; Berger et al., 2008). Lowell (1968) first proposed a conceptual model of the lateral and vertical variations in mineralogy within alteration zones. Some similar models were developed for potassic alteration, which is usually situated in the center and deep parts of porphyry ore deposits, based on this conceptual model (Sillitoe and Gappe, 1984; Cox and Singer, 1986; Melfos et al., 2002). Fluid inclusion and stable isotope studies are other methods used to outline different mineralization phases based on thermometric and isotope element parameters and other geological parameters (e.g., Boyce et al., 2007; Faure et al., 2002; Wilson et al., 2007). Drillhole data and logging information, including mineralographical information, host rock changes and alterations are helpful in delineating mineralization zones. Different geological interpretations could be used to detect zone boundaries, which may also lead to different results because the elemental grade distribution may not be taken into consideration.

Non-Euclidean fractal geometry (Mandelbrot, 1983) is an important branch of nonlinear mathematical sciences and has been applied in various research fields of the geosciences since the 1980s. The relationships between geology, geochemistry and mineralogical settings and spatial information can be researched by methods based on fractal geometry (Afzal et al., 2011; Carranza, 2008, 2009). Bolviken et al. (1992) and Cheng et al. (1994) have shown that geochemical patterns of various elements have fractal dimensions. The concentration-area (C-A) model was proposed by Cheng et al. (1994) to recognize geochemical anomalies from background concentrations and calculate elemental thresholds of different geochemical data. Furthermore, many other fractal models have been proposed and applied in geochemical exploration work, including the number-size (N-S) fractal model proposed by Mandelbrot (1983) and Agterberg (1995), the power spectrum-area (S-A) fractal model proposed by Cheng et al. (1999), the concentration-distance (C-D) fractal model proposed by Li et al. (2003), the concentration-volume (C-V) fractal model proposed by Afzal et al. (2011) and the power spectrum-volume (S-V) fractal model proposed by Afzal et al. (2012).

Methods of fractal analysis also illustrate the relationships between geological, geochemical and mineralogical settings and spatial information derived from the analysis of mineral deposit occurrence data (Carranza, 2008; Carranza et al., 2009; Goncalves et al., 2001). Various geochemical processes can be described based on the differences in fractal dimensions obtained from the analysis of relevant geochemical data. Afzal et al. (2011) considered that the log-log plots obtained by fractal methods are useful tools to delineate different geological populations of geochemical data, and the thresholds could be determined as some breakpoints in those plots.

The application of fractal models to delineate various grade mineralization zones was dependent on the relationships between the metal grades and volumes (Afzal et al., 2011; Agterberg et al., 1993; Cheng, 2007; Sim et al., 1999; Turcotte, 1986). Afzal et al. (2011 and 2012) proposed a concentration-volume (C-V) and power spectrum-volume (S-V) fractal model to delineate different porphyry-Cu mineralized zones and barren host rocks. In this paper, N-S, C-V and S-V fractal models were applied to delineate various mineralized zones and barren host rocks in the Pulang porphyry copper deposit, Yunnan, Southwest China.

2. Fractal models

2.1. Number-size (N-S) fractal model

The number-size (N-S) method proposed by Mandelbrot (1983) can be utilized to describe the distribution of geochemical populations (Sadeghi et al., 2012). In this method, geochemical data does not undergo any preprocessing (Mao et al., 2004). This model shows a relationship between desirable attributes (e.g., Cu concentration in this study) and their cumulative number of samples (Sadeghi et al., 2012). A power-law frequency model has been proposed to explain the N-S relationship according to the frequency distribution of elemental concentrations and cumulative number of samples with those attributes (e.g., Li et al., 1994; Sadeghi et al., 2012; Sanderson et al., 1994; Shi and Wang, 1998; Turcotte, 1996; Zuo et al., 2009a).

The N-S model proposed by Mandelbrot (1983) can be expressed as follows:

$$N(\geq\rho)=F\rho^{-D} \tag{1}$$

where ρ denotes the element concentration, $N(\geq\rho)$ denotes the cumulative number of samples with concentrations greater than or equal to ρ, F is a constant and D is the scaling exponent or fractal dimension of the distribution of element concentrations. According to Mandelbrot (1983), log-log plots of $N(\geq\rho)$ versus ρ show linear segments with different slopes -D corresponding to different concentration intervals.

2.2. Concentration-volume (C-V) fractal model

Afzal et al. (2011) proposed a concentration-volume (C-V) fractal model based on the same principle of the concentration-area (C-A) model (Cheng et al., 1994) to analyze the relationship between the concentration of ore elements and accumulative volume with concentrations greater than or equal to a given value (Afzal et al., 2011; Zuo et al., 2016; Lin et al., 2013; Sadeghi et al., 2012; Soltani et al., 2014; Sun and Liu, 2014; Wang, G. et al., 2012). This model can be expressed as follows:

$$V(\rho \leq \upsilon) \propto \rho^{-a_1}; \; V(\rho \geq \upsilon) \propto \rho^{-a_2} \quad (2)$$

$V(\rho \geq \upsilon)$ and $V(\rho \leq \upsilon)$ represent the occupied volumes with concentrations above or equal to and less than or equal to the contour value υ; υ indicates the threshold value of a zone; and a_1 and a_2 are the characteristic indexes. The thresholds obtained by this method indicate the boundaries between the different grade mineralization zones and barren host rocks of ore deposits. The drillhole data of the elemental concentrations were interpolated by using geostatistical estimation to compute $V(\rho \geq \upsilon)$ and $V(\rho \leq \upsilon)$, which are the volume values enclosed by a contour level ρ in a 3D model.

2.3. Power spectrum-volume (S-V) fractal model

Different geochemical patterns in the spatial domain could be seen as layered signals of various frequencies. Cheng et al. (1999) proposed the power spectrum-area (S-A) fractal model to recognize geochemical anomalies from backgrounds utilizing the method of spectrum analysis in the frequency domain according to this argument. This model is combined with a concentration-area (C-A) model (Cheng et al. 1994), offering a useful tool to determine an optimum threshold value between various patterns based on the scaling property.

Afzal et al. (2012) proposed the power spectrum-volume (S-V) fractal model to delineate different grade mineralization zones based on the same principle as the S-A model proposed by Cheng et al. (1999). The S-V model was utilized in the frequency domain by applying a fast Fourier transformation to the assay data. The straight lines obtained by log-log plotting indicate the relationships between the power spectra and relevant volumes of ore elements. These relationships were utilized to recognize the hypogene zones and supergene enrichment zones from the barren host rocks and the leached zone of the deposit. The recognition of various mineralization zones is based on the power-law relationships between the power spectra and occupied volumes. The formula is as follows:

$$V(\geq S) \propto S^{-2/\beta} \quad (3)$$

where the power-law relationships between the power spectra ($S=-\|F(Wx, Wy, Wz)\|$) and occupied volumes with power spectra greater than or equal to S can be indicated by this form; F represents the fast Fourier transformation of the measurement $\mu(x, y, z)$; and Wx, Wy and Wz indicate wave numbers or angular frequencies in the X, Y and Z directions in a 3D model. The range of index β is $0<\beta\leq2$ or $1\leq2/\beta$ with the special cases of $\beta=2$ and $2/\beta=1$ corresponding to nonfractal and monofractal expressions, and $1<2/\beta$ corresponding to multifractals (Cheng, 2006).

By using the method of geostatistical estimation, the drillhole data of elemental concentration values were interpolated to construct a block model of ore element distribution. The power spectrum values can be obtained by 3D fast Fourier transformation of the ore element grades. The logarithm of all the power spectrum values and accumulative volume values were calculated. Additionally, the log-log plot between power spectrum and volume was drawn according to previously determined values. Then, the filters were constructed on the basis of threshold values obtained by the log-log plot of S-V. Finally, the power spectra were converted back to the space domain by utilizing inverse fast Fourier transformation.

3. Geological setting of the Pulang porphyry copper deposit

The Pulang porphyry copper deposit is situated in the southern end of the Yidun continental arc, Southwest China (Fig. 1). The continental arc was produced due to the westward subduction of Garze–Litang oceanic crust (Deng et al., 2014b, 2015; Wang et al., 2014). The Pulang ore deposit, one of the largest porphyry copper deposits in China (Deng et al., 2012, 2014a; Mao et al., 2012, 2014), is characterized by a typical porphyry-type alteration zone. The geological characteristics of the deposit, including the alteration types and their zonation, the geometry of the orebody, the metallogenic time and the geodynamic settings, have been systematically researched (Leng et al., 2012; Li et al., 2011, 2013). The deposit consists of five ore-bearing porphyry bodies covering an area of approximately 9 km^2, and the explored ore tonnage of Cu is estimated to be 6.50 Mt (Liu et al., 2013).

The outcrop strata of the Pulang deposit are dominated by Upper Triassic Tumugou Formation clastic rocks and andesite and Quaternary sediments (Fig. 1c). The Triassic porphyry intrusions primarily comprise quartz diorite porphyry, quartz monzonite porphyry, quartz diorite porphyrite and granodiorite porphyry. The Tumugou Formation strata were intruded by the quartz diorite porphyry with an age of 219.6 ± 3.5 Ma (zircon U-Pb dating) (Pang et al., 2009). Then, quartz monzonite porphyry with an age of 212.8 ± 1.9 Ma and granodiorite porphyry with an age of 206.3 ± 0.7 Ma (zircon U-Pb dating) (Liu et al., 2013) crosscut the quartz diorite porphyry. The quartz monzonite porphyry is considered to be associated with mineralization because its age is similar to the molybdenite Re-Os isochron age of 213 ± 3.8 Ma from the orebody (Zeng et al., 2004). Moreover, the Cu concentrations of the quartz monzonite porphyry are higher than those of the other porphyries.

The porphyry-type alteration zones transition from early potassium-silicate alteration through quartz-sericite alteration to propylitization, upward and outward from the core of the quartz monzonite porphyry (Fig. 4). The wall rocks near the porphyries were mostly changed into hornfels. Systematic drilling has demonstrated that the potassium-silicate and quartz-sericite zones host the main orebodies, constituting the core of mineralized zones. The propylitic zones and hornfels only develop weak mineralization. The orebodies occur mainly in potassium-silicate and quartz-sericite and occur as veins in the propylitic zones and hornfels. The major rock types in the deposit are quartz monzonite porphyry, quartz diorite porphyrite, granite diorite porphyry, quartz diorite porphyry and hornfels (Fig. 2). Metallic minerals mainly include pyrite, chalcopyrite with a small amount of molybdenite and pyrrhotite (Fig. 3).

4. Fractal modeling

Based on the geological data (which include the collar coordinates of each drillhole, azimuth and dip (orientation), lithology and mineralogy) recorded from 130 drillholes in the Pulang deposit, 20492 lithogeochemical samples were collected at 2 m intervals. The laboratory of the 3rd Geological Team of the Yunnan Bureau of Geology and Mineral Resources utilized the iodine-fluorine and oscillo polarographic method to analyze the concentrations of Cu and associated paragenetic elements, and its analytical uncertainty is less than 7% (Yunnan Diqing Nonferrous Metal Co. Ltd., 2009). Only Cu concentrations were studied in this study. The histogram and Q-Q plot of the log-transformed Cu data indicate that the distribution of Cu data is log-normal (Fig. 5). The experimental semivariogram of the Cu data of the Pulang deposit indicates a range and nugget effect of 320.0 m and 0.25, respectively (Fig. 6). The spherical model is fitted with regard to the experimental semivariogram. The 3D model of the Cu concentration distribution of the Pulang deposit was produced with the ordinary kriging method using Geovia Surpac software on the basis of the semivariogram and anisotropic ellipsoid. Fundamentally, the accuracy of the interpolation results mainly depends on whether the interpolation model accurately fits the spatial distribution characteristics of the deposit. Ordinary kriging was used because it is compatible with a stationary model; it only requires a variogram, and it is the most commonly used form of kriging (Chilès and Delfiner, 1999). Goovaerts (1997) showed that the values in unsampled locations are estimated by the ordinary kriging method according to the moving average of the interest variables, satisfying various distribution forms of data. Ordinary kriging is a spatial estimation method in which the error variance is minimized. This error variance is based on the configuration of the data and its variogram (Yamamoto, 2005). The correct variogram in kriging interpolation can guarantee the accuracy of the interpolation results.

The accuracy of the spatial interpolation analysis is verified by comparing the difference between the measured values and the predicted values to select the best variogram model. To test the variogram model, the cross-validation method was used to determine whether the parameters of the variogram model were correct. The distribution of the residual is normal (Fig. 7), and the mean error between the actual and estimated Cu grades is equal to 0 (Table 1). This result indicates that this model is reasonable and that the variogram parameters used for estimating the Cu grade are unbiased.

The obtained block models were used as inputs to the fractal models. The Pulang deposit was modeled by 20 m×20 m×5 m voxels, and they were decided by the grid drilling dimensions and geometrical properties of the deposit (David, 1970). The Pulang deposit is totally modeled with 150973 voxels. The terms “highly”, "moderately" and "weakly" have been used to classify mineralized zones based on fractal modeling, in accordance with the classification of the ore grades in the deposit.

4.1. Number-size (N-S) fractal modeling

The N-S model was applied to the Cu data (Fig. 8). The selection of breakpoints as threshold values is an objective decision because geochemical populations are defined by different line segments in the N-S log-log plot. The straight fitted lines were obtained based on least-square regression (Agterberg et al., 1996; Spalla et al., 2010). In other words, the intensity of element enrichment is depicted by each slope of the line segments in the N-S log-log plots (Afzal et al., 2010; Bai et al., 2010).

Based on the classification of the 3D model of Cu data and the thresholds obtained from the N-S fractal model (Table 2), highly mineralized zones are situated in the southern and central parts of the Pulang deposit and coincide with the potassium-silicate alterations. However, small and highly mineralized zones are located in the central parts of the Pulang deposit (Fig. 9). Moderately mineralized zones occur along a northwest-southeast trend and correlate with the phyllic zones. Weakly mineralized zones and barren host rocks are situated in the marginal parts of the area.

4.2. Concentration-volume (C-V) fractal modeling

The occupied volumes corresponding to the Cu grades were computed to obtain the concentration-volume model according to the 3D model of the Pulang deposit. Through the obtained C-V log-log plot, the threshold values of the Cu grades were determined (Fig. 10). These results indicate the power-law relationship between Cu grade and volume. According to these results (Table 3), the low-concentration zones exist in many parts of the deposit and occur along a northwest-southeast trend. Moderately and highly mineralized zones are situated in several parts of the central deposit and to the south of the deposit (Fig. 11).

4.3. Power spectrum-volume (S-V) fractal modeling

Based on the geological data (which include the collar coordinates of each drillhole, azimuth and dip (orientation), lithology and mineralogy) recorded from 130 drillholes in the deposit, a 3D model and block model of the distribution of Cu in the Pulang deposit were constructed with ordinary kriging using Geovia Surpac software.

The power spectrum (S) was calculated for the 3D elemental distribution using 3D fast Fourier transformation in MATLAB (R2016a). The logarithmic values of the power spectra and relevant volumes were plotted against each other (Fig. 12). The straight lines fitted in the log-log plot indicate different relationships between the power spectra and occupied volumes. The thresholds of logS = 7.81 and logS = 8.70 were determined by the log-log S-V plot. The 3D filters were designed to separate different mineralization zones on the basis of these threshold values. Inverse fast Fourier transformation was used to convert the decomposed components back into the space domain by using MATLAB (R2016a). According to the results, the Cu concentrations of the hypogene zones range from 0.23% to 1.33% (Table 4), and values of >1.33% Cu correspond to the supergene enrichment zones, whereas values of <0.23% Cu correspond to the leached zone and barren host rocks (Fig. 13).

5. Comparison of the fractal models and geological model of the deposit

Alteration models have a key role in zone delineation and in presenting geological models, as described by Lowell and Guilbert (1970). The potassic and phyllic alterations control major mineralization within supergene enrichment and hypogene zones according to these models. Models of Cu mineralization zones derived via fractal models can be compared with geological data to validate the results of analysis in different porphyry Cu deposits. The results of the fractal modeling of the Pulang deposit were compared with the 3D geological model of the deposit constructed by using Geovia Surpac and drillhole data (Fig. 2). Moreover, the results obtained from these fractal models were controlled by mineralogical investigations.

Carranza (2011) has illustrated an analysis for the calculation of spatial correlations between two binary datasets, especially mathematical and geological models. An intersection operation between the mineralization zones obtained from fractal models and the different alteration zones in the geological model was performed to derive the amount of voxels corresponding to each of the classes of overlap zones (Table 5). Using the obtained numbers of voxels, the Type I error (T1E), Type II error (T2E), and overall accuracy (OA) of the fractal model were estimated with respect to different alteration zones and the geological data (Carranza, 2011). The OAs of the fractal models of the mineralized zones were compared as follows.

A comparison between highly mineralized zones based on the fractal models and potassic alteration zones resulting from the 3D geological model shows that there is a similarity among these fractal models. The overall accuracies for the C-V, N-S and S-V models are 0.50, 0.51 and 0.52, respectively (Table 6), which indicate that the S-V model gives better results for identifying highly mineralized zones in the deposit. The number of overlapped voxels (A) in the S-V model is higher than those in the N-S and C-V models. The correlation (from OA results) between highly mineralized zones obtained from S-V modeling and potassic alteration zones is better than that of the N-S and C-V model because of a strong proportional relationship between the extension and positions of voxels in the S-V model and the potassic alteration zones in the 3D geological model.

A comparison between phyllic alteration zones resulting from the 3D geological model and moderately and weakly mineralized zones from the fractal modeling shows that the overall accuracies of the C-V, N-S and S-V fractal models with respect to phyllic alteration zones of the geological model are 0.59, 0.54 and 0.56, respectively. The overall accuracy of moderately and weakly mineralized zones obtained from C-V modeling is higher than that of mineralized zones obtained from N-S and S-V modeling (Table 7). On the other hand, moderately mineralized zones defined by C-V modeling overlap with phyllic zones defined by the 3D geological model. However, the results of the C-V model are more accurate than those of the N-S and S-V models with respect to the phyllic zones defined by the 3D geological model.

It could be considered that there are spatial correlations between different modeled Cu zones and geological features such as alterations and mineralogy. Several samples were collected from different drillholes in different grade mineralization zones of the Pulang deposit to validate the results of the fractal models. These samples were analyzed by microscopic identification and XRF (X-ray fluorescence spectrometry). The PL-B82 sample was collected from the drillhole situated in a high-grade mineralization zone and includes a high chalcopyrite content and some molybdenite (Fig. 16a). The PL-B62 sample was collected from the drillhole situated in a moderate-grade mineralization zone and includes a low chalcopyrite content and some pyrrhotite in the polished section (Fig. 16b). The PL-B74 sample was collected from the drillhole located in a weakly mineralized zone with lower chalcopyrite content and some pyrrhotite (Fig. 16c and Fig. 16d). The results obtained from the mineralogy, microscopic identification and drillhole scanning by XRF of these samples indicate that the Cu concentrations are 1.80%, 1.32% and 0.41% in the PL-B82, PL-B62 and PL-B74 samples, respectively (Table 8).

6. Conclusions

In many cases, drillhole logging is dealing with the lack of proper diagnosis of geological phenomena, which can undermine the delineation of mineralized zones because it depends on the subjective interpretation of individual loggers, and no two loggers provide the same interpretations. However, conventional geological modeling based on drillhole data is fundamentally important for understanding the orebody spatial structure. Grades of ore elements are not determined by conventional methods of geological ore modeling, while the variation in ore grades in a mineral deposit is an obvious and salient feature. Given the problems mentioned above, using a series of newly established methods based on mathematical analyses such as fractal modeling seems to be inevitable.

In this paper, the number-size (N-S), concentration-volume (C-V) and power spectrum-volume (S-V) fractal models were used to delineate and recognize various Cu mineralized zones of the Pulang porphyry copper deposit in the southern end of the Yidun continental arc, Southwest China. All these fractal models reveal that high-grade Cu mineralized zones are situated in the central and southern parts of the deposit. The Cu threshold values of highly mineralized zones are 1.45% and 1.88% based on the N-S and C-V fractal models. The Cu threshold of supergene enrichment zones is 1.33% based on the S-V fractal model. The models of moderately mineralized zones contain 0.28-1.45% Cu according to the N-S model and 1.48-1.88% Cu according to the C-V model. The hypogene zones contain 0.23-1.33% Cu according to the S-V model. The N-S model reveals weakly mineralized zones and barren host rocks containing <0.28% Cu. In contrast, the C-V model reveals that the barren host rocks contain <0.25% and that the weakly mineralized zones contain 0.25-1.48% Cu. The S-V model reveals that the barren host rock and leached zone contain <0.23% Cu.

The comparison between highly mineralized zones based on the fractal models and potassic zones resulting from the 3D geological model illustrates that the S-V fractal model is better than the N-S and C-V model because the number of overlapped voxels (A) in the S-V model is higher than those in the N-S and C-V model. The overall accuracies for the C-V, N-S and S-V models are 0.50, 0.51 and 0.52, respectively (Table 6), which indicates that the S-V model gives the best results for identifying highly mineralized zones in the deposit. On the other hand, the correlation (from OA results) between the highly mineralized zones obtained from S-V modeling and the potassic alteration zones is better than those of the N-S and C-V models because of a strong proportional relationship between the extension and positions of the voxels in the S-V model and potassic alteration zones in the 3D geological model.

A comparison between phyllic alteration zones obtained from the 3D geological model and moderate grade mineralization zones obtained from the fractal models indicates that the OA values of the C-V, N-S and S-V fractal methods in reference to the phyllic alteration zones of the geological model are 0.59, 0.54 and 0.56, respectively. The overall accuracy of the moderately and weakly mineralized zones obtained from C-V modeling is higher than the mineralized zones obtained from N-S and S-V modeling (Table 7).

According to the correlation between the results driven by fractal modeling and geological logging from drillholes in the Pulang porphyry copper deposit, high-grade mineralization zones generated by fractal models, especially the S-V model, have a better correlation with potassic alteration zones resulting from the 3D geological model than from the N-S and C-V models. The highly and moderately mineralized zones obtained from the fractal models are both situated in the southern and central parts of the Pulang deposit and coincide with potassic and phyllic alteration zones. There is a better relationship between the moderately and weakly mineralized zones derived by the C-V model and the phyllic alteration zones from the 3D geological model than those derived by the N-S and S-V models.

Acknowledgements

This research was supported by the National Key R&D Program of China (2016YFC0600508). The authors thank Tao Dong, Haijun Yu, Qiwu Shen, Zhipeng Li, Baosheng Shi and Jinhong Yang for supporting in field investigation and providing parts of raw data.

References

Agterberg, F.P., Cheng, Q., and Wright, D.F.: Fractal modeling of mineral deposits, in: Proceedings of the 24th APCOM Symposium, Montreal, Canada, 43–53, 1993.

Agterberg, F.P.: Multifractal modeling of the sizes and grades of giant and sup ergiant deposits, International Geology Review, 37, 1–8, https://doi.org/10.1080/00206819509465388, 1995.

Agterberg, F.P., Cheng, Q., Brown, A., Good, D.: Multifractal modeling of fractures in the Lac du Bonnet batholith, Manitoba. Comput. Geosci. 22, 497–507, 1996.

Afzal, P., Khakzad, A., Moarefvand, P., Rashidnejad Omran, N., Esfandiari, B., Fadakar Alghalandis, Y.: Geochemical anomaly separation by multifractal modeling in Kahang (GorGor) porphyry system, Central Iran. J. Geochem. Explor. 104, 34–46, 2010.

Afzal, P., Fadakar Alghalandis, Y., Khakzad, A., Moarefvand, P., and Rashidnejad Omran, N.: Delineation of mineralization zones in porphyry Cu deposits by fractal concentration–volume modeling, J. Geochem. Explor., 108, 220–232, https://doi.org/10.1016/j.gexplo.2011.03.005, 2011.

Afzal, P., Fadakar Alghalandis, A., Moarefvand, P., Rashidnejad Omran, N., and Asadi Haroni, H.: Application of power–spectrum–volume fractal method for detecting hypogene, supergene enrichment, leached and barren zones in Kahang Cu porphyry deposit, Central Iran, J. Geochem. Explor., 112, 131–138, https://doi.org/10.1016/j.gexplo.2011.08.002, 2012.

Bai, J., Porwal, A., Hart, C., Ford, A., Yu, L.: Mapping geochemical singularity using multifractal analysis: application to anomaly definition on stream sediments data from Funin Sheet, Yunnan, China, J. Geochem. Explor., 104, 1–11, 2010.

Beane, R.E.: Hydrothermal alteration in silicate rocks, in: Advances in Geology of the Porphyry Copper Deposits, Southwestern North America, Titley, S.R. (Ed.), The University of Arizona Press, Tucson, 117–137, 1982.

Bolviken, B., Stokke, P.R., Feder, J., and Jossang, T.: The fractal nature of geochemical landscapes, J. Geochem. Explor., 43, 91–109, 1992.

Boyce, A.J., Fulgnati, P., Sbrana, A., and Fallick, A.E.: Fluids in early stage hydrothermal alteration of high-sulfidation epithermal systems: a view from the volcano active hydrothermal system (Aeolian Island, Italy), Journal of Volcanology and Geothermal Research, 166, 76–90, 2007.

Berger, B. R., Ayuso, R. A., Wynn, J. C., and Seal, R. R.: Preliminary Model of Porphyry Copper Deposits, USGS, Open-File Report, 1321 pp., 2008.

Cox, D. and Singer, D.: Mineral deposits models, US Geological Survey Bulletin, 1693 pp., 1986.

Craig, G.R. and Vaughan, D.: Ore Microscopy and Ore Petrography, John Wile yandSons, 1994.

Chilès, J.P. and Delfiner, P.: Geostatistics: Modeling Spatial Uncertainty, Wiley, NewYork, 695 pp., 1999.

Carranza, E.J.M.: Geochemical Anomaly and Mineral Prospectivity Mapping in GIS. Handbook of Exploration and Environmental Geochemistry, 11, Amsterdam, Elsevier, 351 pp., 2008.

Carranza, E.J.M.: Controls on mineral deposit occurrence inferred from analysis of their spatial pattern and spatial association with geological features, Ore Geol. Rev., 35, 383–400, https://doi.org/10.1016/j.oregeorev.2009.01.001, 2009.

Carranza, E.J.M., Owusu, E.A., and Hale, M.: Mapping of prospectivity and estimation of number of undiscovered prospects for lode gold, southwestern Ashanti Belt, Ghana, Mineralium Deposita, 44, 915–938, https://doi.org/10.1007/s00126-009-0250-6, 2009.

Carranza, E.J.M.: From predictive mapping of mineral prospectivity to quantitative estimation of number of undiscovered prospects. Resource Geology 61, 30–51, 2010.

Carranza, E.J.M.: Analysis and mapping of geochemical anomalies using logratio-transformed stream sediment data with censored values, J. Geochem. Explor., 110, 167–185, https://doi.org/10.1016/j.gexplo.2011.05.007, 2011.

Cheng, Q., Agterberg, F.P., and Ballantyne, S.B.: The separation of geochemical anomalies from background by fractal methods, J. Geochem. Explor., 51, 109–130, https://doi.org/10.1016/0375-6742(94)90013-2, 1994.

Cheng, Q.: Spatial and scaling modelling for geochemical anomaly separation, J. Geochem. Explor., 65, 175–194, https://doi.org/10.1016/S0375-6742(99)00028-X,1999.

Cheng, Q.: Multifractal modelling and spectrum analysis: methods and applications to gamma ray spectrometer data from southwestern Nova Scotia, Canada, Science in China, Series D: Earth Sciences 49 (3), 283–294, 2006.

Cheng, Q.: Mapping singularities with stream sediment geochemical data for prediction of undiscovered mineral deposits in Gejiu, Yunnan Province, China, Ore Geol. Rev., 32, 314–324, https://doi.org/10.1016/j.oregeorev.2006.10.002, 2007.

David, M.: Geostatistical Ore Reserve Estimation, Amsterdam, Elsevier, 283 pp., 1970.

Deng, J., Wang, C.M., and Li, G.J.: Style and process of the superimposed mineralization in the Sanjiang Tethys, Acta Petrologica Sinica, 28 (5), 1349–1361 (in Chinese with English abstract), 2012.

Deng, J., Wang, Q.F., Li, G.J., and Santosh, M.: Cenozoic tectono-magmatic and metallogenic processes in the Sanjiang region, southwestern China, Earth Sci. Rev., 138, 268–299, https://doi.org/10.1016/j.earscirev.2014.05.015, 2014a.

Deng, J., Wang, Q.F., Li, G.J., Li, C.S., and Wang, C.M.: Tethys tectonic evolution and its bearing on the distribution of important mineral deposits in the Sanjiang region, SW China, Gondwana Research, 26 (2), 419–437, https://doi.org/10.1016/j.gr.2013.08.002, 2014b.

Deng, J., Wang, Q.F., Li, G.J., Hou, Z.Q., Jiang, C.Z., and Danyushevsky, L.: Geology and genesis of the giant Beiya porphyry–skarn gold deposit, northwestern Yangtze Block, China, Ore Geol. Rev., 70, 457–485, https://doi.org/10.1016/j.oregeorev.2015.02.015, 2015.

Faure, K., Matsuhisa, Y., Metsugi, H., Mizota, C., and Hayashi, S.: The Hishikari Au–Ag epithermal deposit, Japan: oxygen and hydrogen isotope evidence in determining the source of paleo hydrothermal fluids, Economic Geology, 97, 481–498, https://doi.org/10.2113/gsecongeo.97.3.481, 2002.

Goovaerts, P.: Geostatistics for Natural Resources Evaluation, Oxford University

Press, New York, 496 pp. , 1997.

Goncalves, M. A., Mateus, A., and Oliveira, V.: Geochemical anomaly separation by multifractal modeling, J. Geochem. Explor., 72, 91–114, https://doi.org/10.1016/S0375-6742(01)00156-X, 2001.

Lowell, J.D.: Geology of the Kalamazoo orebody, San Manuel district, Arizona, Economic Geology, 63, 645–654, https://doi.org/10.2113/gsecongeo.63.6.645, 1968.

Lowell, J.D. and Guilbert, J.M.: Lateral and vertical alteration-mineralization zoning in porphyry ore deposits, Economic Geology, 65, 373–408, https://doi.org/10.2113/gsecongeo.65.4.373, 1970.

Li, C., Xu, Y., Jiang, X.: The fractal model of mineral deposits. Geol. Zhejiang 10, 25–32 (In Chinese with English Abstract), 1994.

Li, C., Ma, T., and Shi, J.: Application of a fractal method relating concentrations and distances for separation of geochemical anomalies from background, J. Geochem. Explor., 77, 167–175, https://doi.org/10.1016/S0375-6742(02)00276-5, 2003.

Li, W.C., Zeng, P.S., Hou, Z.Q., and White, N.C.: The Pulang porphyry copper deposit and associated felsic intrusions in Yunnan Province, Southwest China, Economic Geology, 106 (1),79–92, https://doi.org/10.2113/econgeo.106.1.79 , 2011.

Leng, C.B., Zhang, X.C., Hu, R.Z., Wang, S.X., Zhong, H., Wang, W.Q., and Bi, X.W.: Zircon U–Pb and molybdenite Re–Os geochronology and Sr–Nd–Pb–Hf isotopic constraintson the genesis of the Xuejiping porphyry copper deposit in Zhongdian, Northwest Yunnan, China, Journal of Asian Earth Sciences, 60, 31–48, 2012.

Liu, X.L., Li, W.C., Yin, G.H., and Zhang, N.: The geochronology, mineralogy and geochemistry study of the Pulang porphyry copper deposits in Geza arc of Yunnan Province, Acta Petrologica Sinica, 29(9), 3049–3064 (in Chinese with English abstract), 2013.

Mandelbrot, B. B.: The Fractal Geometry of Nature, W. H. Freeman, San Fransisco, 468 pp., 1983.

Melfos, V., Vavelidis, M., Christodes, G., and Seidel, E.: Origin and evolution of the Tertiary Maronia porphyry copper–molybdenum deposit, Thrace, Greece, Mineralium Deposita, 37, 648–668, https://doi.org/10.1007/s00126-002-0277-4, 2002.

Mao, Z., Peng, S., Lai, J., Shao, Y., Yang, B.: Fractal study of geochemical prospecting data in south area of Fenghuanshan copper deposit, Tongling Anhui, J. Earth Sci. Environ, 26, 11–14, 2004.

Mao, J.W., Zhou, Z.H., Feng, C.Y., Wang, Y.T., Zhang, C.Q., Peng, H.J., and Yu, M.: A preliminary study of the Triassic large-scale mineralization in China and its geodynamic setting, Geology in China, 39(6), 1437–1471 (in Chinese with English abstract), 2012.

Mao, J.W., Pirajno, F., Lehmann, B., Luo, M.C., and Berzina, A.: Distribution of porphyry deposits in the Eurasian continent and their corresponding tectonic settings, Journal of Asian Earth Sciences, 79 (PartB), 576–584, https://doi.org/10.1016/j.jseaes.2013.09.002, 2014.

Pang, Z.S., Du, Y.S., Wang, G.W., Guo, X., Cao, Y., and Li, Q.: Single-grain zircon U–Pb isotopic ages, geochemistry and its implication of Pulang complex in Yunnan Province, China, Acta Petrologica Sinica, 25(1), 159–165 (in Chinese with English abstract), 2009.

Pyrcz, M.J. and Deutsch, C.V.: Geostatistical Reservoir Modeling, Oxford University Press, 2014.

Sanderson, D.J., Roberts, S., Gumiel, P.: A fractal relationship between vein thickness and gold grade in drill core from La Codosera, Spain. Econ. Geol., 89, 168–173, 1994.

Schwartz, G.M.: Hydrothermal alteration in the “porphyry copper” deposits, Economic Geology, 42, 319–352, https://doi.org/10.2113/gsecongeo.42.4.319, 1947.

Shi, J., Wang, C.: Fractal analysis of gold deposits in China: implication for giant deposit exploration. Earth Sci. J. China Univ. Geosci. 23, 616–618 (In Chinese with English abstract), 1998.

Sillitoe, R.H. and Gappe, I.M.: Philippine porphyry copper deposits: geologic setting and characteristics, Common Coordination Joint Resource (CCOP), 14, 1–89, 1984.

Sillitoe, R.H.: Characteristics and controls of the largest porphyry copper–gold and epithermal gold deposits in the circum-pacific region, Australian Journal of Earth Sciences, 44, 373–388, https://doi.org/10.1080/08120099708728318, 1997.

Sim, B.L., Agterberg, F.P., and Beaudry, C.: Determining the cutoff between background and relative base metal contamination levels using multifractal methods, Comput. Geosci., 25, 1023–1041, 1999.

Sadeghi, B., Moarefvand, P., Afzal, P., Yasrebi, A.B., and Saein, L.D.: Application of fractal models to outline mineralized zones in the Zaghia iron ore deposit, Central Iran, J. Geochem. Explor., 122, 9–19, https://doi.org/10.1016/j.gexplo.2012.04.011, 2012.

Soltani, F., Afzal, P., and Asghari, O.: Delineation of alteration zones based on Sequential Gaussian Simulation and concentration–volume fractal modeling in the hypogene zone of Sungun copper deposit, NW Iran, J. Geochem. Explor., 140, 64–76, https://doi.org/10.1016/j.gexplo.2014.02.007, 2014.

Spalla, M.I., Morotta, A.M., Gosso, G.: Advances in interpretation of geological processes: refinement of multi-scale data and integration in numerical modelling. Geological Society, London, 240 pp, 2010.

Sun, T. and Liu, L.: Delineating the complexity of Cu-Mo mineralization in a porphyry intrusion by computational and fractal modeling: A case study of the Chehugou deposit in the Chifeng district, Inner Mongolia, China, J. Geochem. Explor., 144, 128–143, https://doi.org/10.1016/j.gexplo.2014.02.015, 2014.

Turcotte, D.L.: A fractal approach to the relationship between ore grade and tonnage, Economic Geology, 18, 1525–1532, 1986.

Turcotte, D.L.: Fractals in geology and geophysics, Pure Appl. Geophys., 131, 171–196, 1989.

Turcotte, D.L.: Fractals and Chaos in Geophysics. second ed. Cambridge University Press, Cambridge UK, pp. 81–99, 1996.

White, N.C. and Hedenquist, J.W.: Epithermal gold deposits: styles, characteristics and exploration, SEG Newsletter, 23, 1–14, 1995.

Wilson, A.J., Cooke, David, R., Harper, B.J., and Deyell, C.L.: Sulfur isotopic zonation in the Cadia district, southeastern Australia: exploration significance and implications for the genesis of alkalic porphyry gold–copper deposits, Mineralium Deposita, 42, 465–487, https://doi.org/10.1007/s00126-006-0071-9, 2007.

Wang, Q.F., Deng, J., Liu, H., Wang, Y., Sun, X., and Wan, L.: Fractal models for estimating local reserves with different mineralization qualities and spatial variations, J. Geochem. Explor., 108, 196–208, https://doi.org/10.1016/j.gexplo.2011.02.008, 2011.

Wang, Q.F., Deng, J., Li, C.S., Li, G.J., Yu, L., and Qiao, L.: The boundary between the Simao and Yangtze blocks and their locations in Gondwana and Rodinia: constraints from detrital and inherited zircons, Gondwana Research, 26(2), 438–448, https://doi.org/10.1016/j.gr.2013.10.002, 2014.

Wang, G. W., Emmanuel John M. Carranza, Zuo, R., Hao, Y. L., Du, Y. S., Pang, Z. S., and Sun Y.: Mapping of district-scale potential targets using fractal models, J. Geochem. Explor., 122, 34–46, https://doi.org/10.1016/j.gexplo.2012.06.013, 2012.

Yamamoto, J.K.: Comparing Ordinary Kriging Interpolation Variance and Indicator Kriging Conditional Variance for Assessing Uncertainties at Unsampled Locations, in: Application of Computers and Operations Research in the Mineral Industry, edited by: Dessureault, S., Ganguli, R., Kecojevic, V., and Girard-Dwyer, J., Balkema, 2005.

Yunnan Diqing Nonferrous Metal Co. Ltd.: Exploration Report of Pulang Copper Deposit, Diqing, Yunnan, China, Yunnan Diqing Nonferrous Metal Co. Ltd., Diqing Tibetan Autonomous Prefecture (in Chinese), 2009.

Zeng, P.S., Hou, Z.Q., Li, L.H., Qu, W.J., Wang, H.P., Li, W.C., Meng, Y.F., and Yang, Z.S.: Age of the Pulang porphyry copper deposit in NW Yunnan and its geological significance, Geological Bulletin of China, 23(11), 1127–1131 (in Chinese with English abstract), 2004.

Zuo, R., Cheng, Q., and Xia, Q.: Application of fractal models to characterization of vertical distribution of geochemical element concentration, J. Geochem. Explor., 102, 37–43, https://doi.org/10.1016/j.gexplo.2008.11.020, 2009.

Zuo, R. and Wang, J.: Fractal/multifractal modeling of geochemical data: A review, J. Geochem. Explor., 164, 33-41, https://doi.org/10.1016/j.gexplo.2015.04.010, 2016.

Fig.1. Geological map of the Pulang porphyry copper deposit, SW China. Modified after Yunnan Diqing Nonferrous Metal Co. Ltd., 2009.

Fig.2. Geological 3D models including lithology, alteration and 3D drill hole plot with the legend of each in the Pulang porphyry copper deposit. (Scale is in m^3.)

Fig.3. Photographs of alteration and mineralization in the Pulang porphyry copper deposit, SW China. (a) Quartz monzonite porphyry with potassium-silicate alteration; (b) Quartz diorite porphyrite with quartz-sericite alteration; (c) Quartz diorite porphyrite with propylitic alteration; (d) Hornfels. Qtz=quartz; Pl=plagioclase; Kfs=K-feldspar; Bt=biotite; Ser=sericite; Chl=chlorite; Ep=epidote; Py=pyrite; Ccp=chalcopyrite; Mo=molybdenite; Po= pyrrhotite.

Fig.4. Cross section along exploration line 0 in the Pulang porphyry copper deposit, SW China. Modified after Wang et al., 2012.

Fig.5. Histograms of (a) the Cu raw and (b) logarithmic transformation data and (c) Q-Q plot of the log-transformed Cu data in the Pulang deposit.

Fig.6. The experimental semivariogram (omni-directional) of Cu data in Pulang deposit.

Fig.7. The cross-validation results: (a) residual VS Cu grade; (b) the residual d istribution histogram.

Fig.8. N–S log–log plot for Cu concentrations in the Pulang deposit.

Fig.9. Zones in the Pulang deposit based on thresholds defined from the N–S fractal model of Cu data: (a) highly mineralized zones; (b) moderately mineralized zones; (c) weakly mineralized zones and barren host rocks. (Scale is in m^3.)

Fig.10. C–V log–log plot for Cu concentrations in the Pulang deposit.

Fig.11. Zones in the Pulang deposit based on thresholds defined from the C–V fractal model of Cu data: (a) highly mineralized zones; (b) moderately mineralized zones; (c) weakly mineralized zones; (d) barren host rock.(Scale is in m^3.)

Fig.12. S–V log–log plot for Cu concentrations in the Pulang deposit.

Fig.13. Zones in the Pulang deposit based on thresholds defined from the S–V fractal model of Cu data: (a) the supergene enrichment zones; (b) the hypogene zones; (c) the leached zone and barren host rock (Scale is in m^3.)

Fig.14. Highly mineralized zones in the Pulang deposit: (a) potassium-silicate zone resulted from the 3D geological model from drillhole geological data; (b) N–S modeling of Cu data; and (c) C–V modeling of Cu data; (d) S–V modeling of Cu data (Scale is in m^3.)

Fig.15. Moderately mineralized zones in the Pulang deposit:(a) quartz–sericite zones resulted from the 3D geological model from drillhole geological data; (b) N–S modeling of Cu data; and (c) C–V modeling of Cu data; (d) S–V modeling of Cu data (Scale is in m^3.)

Fig.16. Chalcopyrite content in several samples based on mineralographical study: (a) PL-B82 sample was collected from the drillhole situated in the high grade mineralization zones.; (b) PL-B62 sample was collected from the drillhole situated in the moderately grade mineralization zones.; (c) and (d) PL-B74 sample was collected from the drillhole located at the weakly mineralized zones.

Table 1 The results of statistical characteristics of the residual.

Table 2 Thresholds concentrations obtained by using N-S model based on Cu% in Pulang deposit.

Table 3 Thresholds concentrations obtained by using C-V model based on Cu% in Pulang deposit.

Table 4 Ranges of power spectrum (S) for different mineralization zones in Pulang deposit.

Table 5 Matrix for comparing performance of fractal modeling results with geological model. A, B, C, and D represent number of voxels in overlaps between classes in the binary geological model and the binary results of fractal models (Carranza, 2011).

Table 6 Overall accuracy (OA), Type I and Type II errors (T1E and T2E, respectively) with respect to potassic alteration zone resulted from geological model and threshold values of Cu obtained through C–V , N–S and S–V fractal modeling.

Table 7 Overall accuracy (OA), Type I and Type II errors (T1E and T2E, respectively) with respect to phyllic alteration zone resulted from geological model and threshold values of Cu obtained through C–V, N–S and S–V fractal modeling.

Table 8 Results of XRF analysis of samples collected from different mineralized zones in the Pulang porphyry copper deposit.

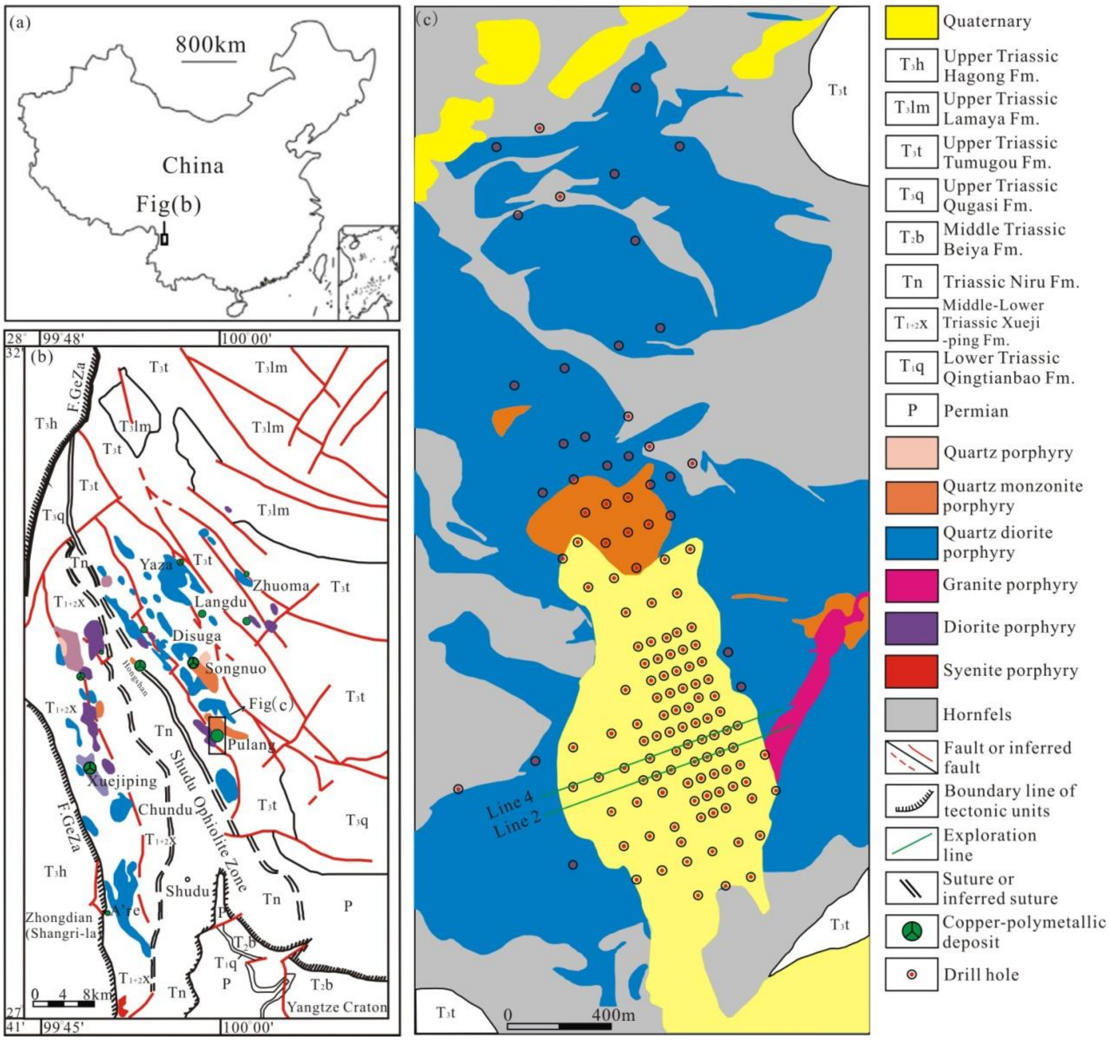
(a)
800km
China
Fig(b)
(b)
28°32'
99°48'
100°00'
27°41'
99°45'
F.GeZa
T3h
T3t
T3lm
T3q
Tn
T1+2x
Yaza
Zhuoma
Langdu
Disuga
Songnuo
Fig(c)
Pulang
Xuejiping
Chundu
Shudu
Shudu Ophiolite Zone
Hongshan
A're
Zhongdian (Shangri-la)
T2b
T1q
P
Yangtze Craton
0 4 8km
(c)
Line 4
Line 2
0 400m
Quaternary
Upper Triassic Hagong Fm.
Upper Triassic Lamaya Fm.
Upper Triassic Tumugou Fm.
Upper Triassic Qugasi Fm.
Middle Triassic Beiya Fm.
Triassic Niru Fm.
Middle-Lower Triassic Xueji-ping Fm.
Lower Triassic Qingtianbao Fm.
Permian
Quartz porphyry
Quartz monzonite porphyry
Quartz diorite porphyry
Granite porphyry
Diorite porphyry
Syenite porphyry
Hornfels
Fault or inferred fault
Boundary line of tectonic units
Exploration line
Suture or inferred suture
Copper-polymetallic deposit
Drill hole

Fig. 1.

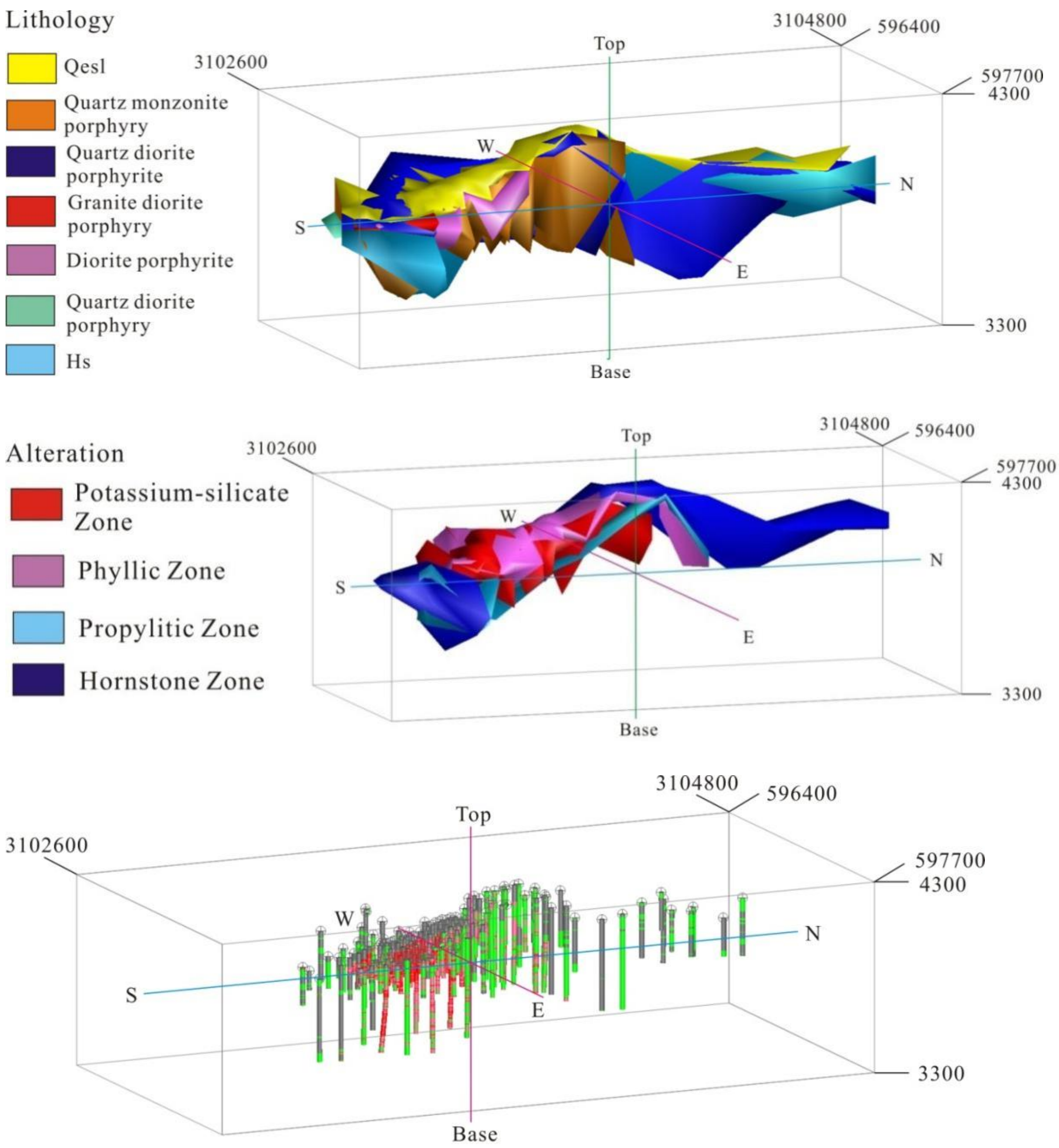
Lithology
Qesl
Quartz monzonite porphyry
Quartz diorite porphyrite
Granite diorite porphyry
Diorite porphyrite
Quartz diorite porphyry
Hs
3102600
3104800
596400
597700
4300
3300
Top
Base
W
E
S
N
Alteration
Potassium-silicate Zone
Phyllic Zone
Propylitic Zone
Hornstone Zone

Fig. 2.

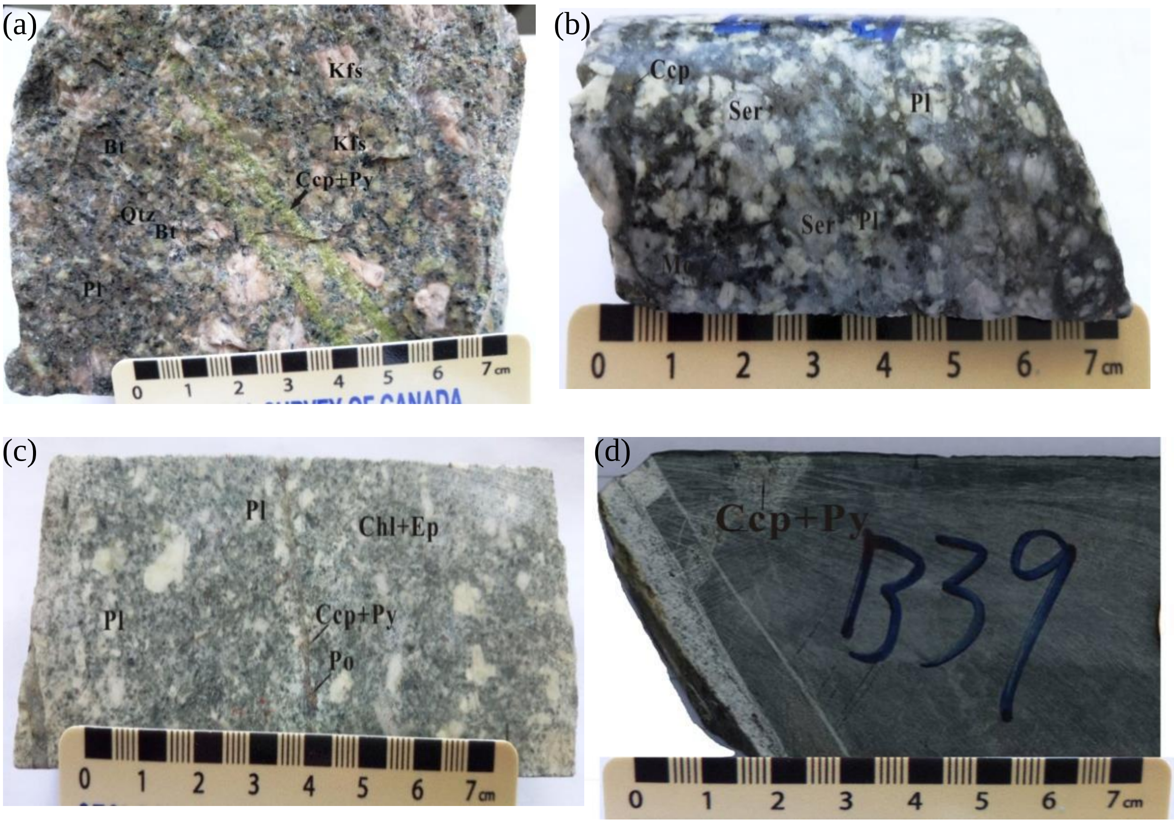
(a)
Kfs
Bt
Kfs
Ccp+Py
Qtz
Bt
Pl
(b)
Ccp
Ser
Pl
Ser
Pl
(c)
Pl
Chl+Ep
Pl
Ccp+Py
Po
(d)
Ccp+Py
B39

Fig. 3.

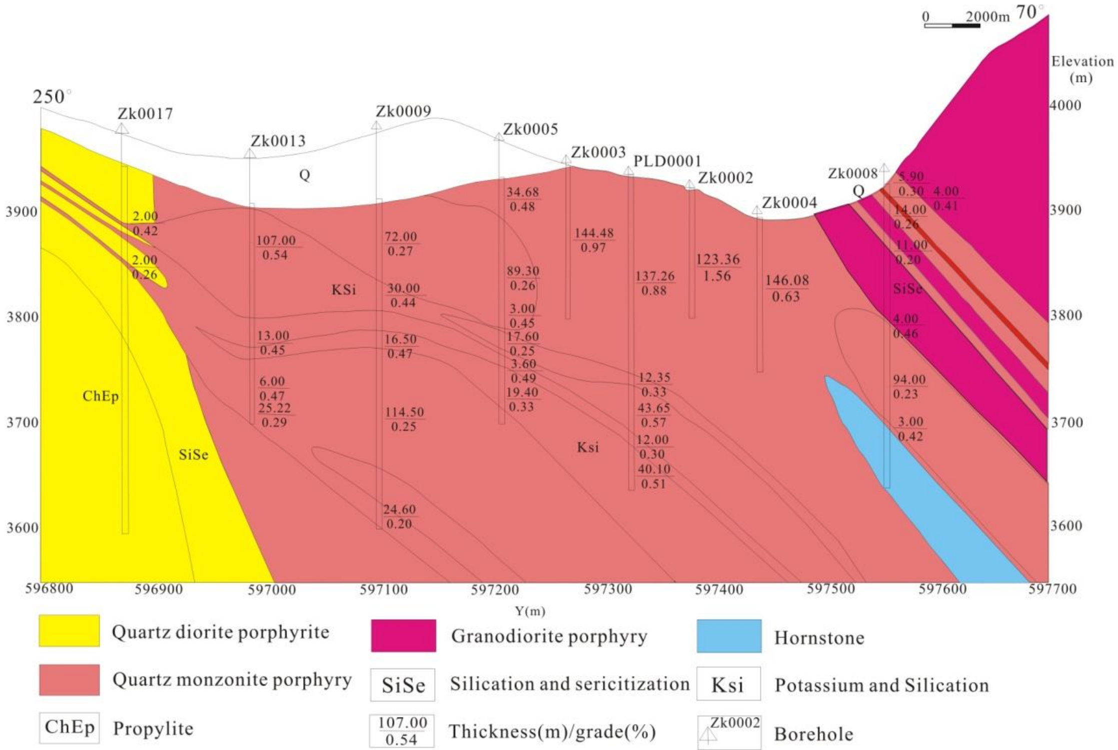
0 2000m
250°
70°
Elevation (m)
Zk0017
Zk0013
Zk0009
Zk0005
Zk0003
PLD0001
Zk0002
Zk0004
Zk0008
Q
KSi
Ksi
ChEp
SiSe
4000
3900
3800
3700
3600
596800
596900
597000
597100
597200
597300
597400
597500
597600
597700
Y(m)
Quartz diorite porphyrite
Granodiorite porphyry
Hornstone
Quartz monzonite porphyry
SiSe Silication and sericitization
Ksi Potassium and Silication
ChEp Propylite
107.00 0.54 Thickness(m)/grade(%)
Zk0002 Borehole

Fig. 4.

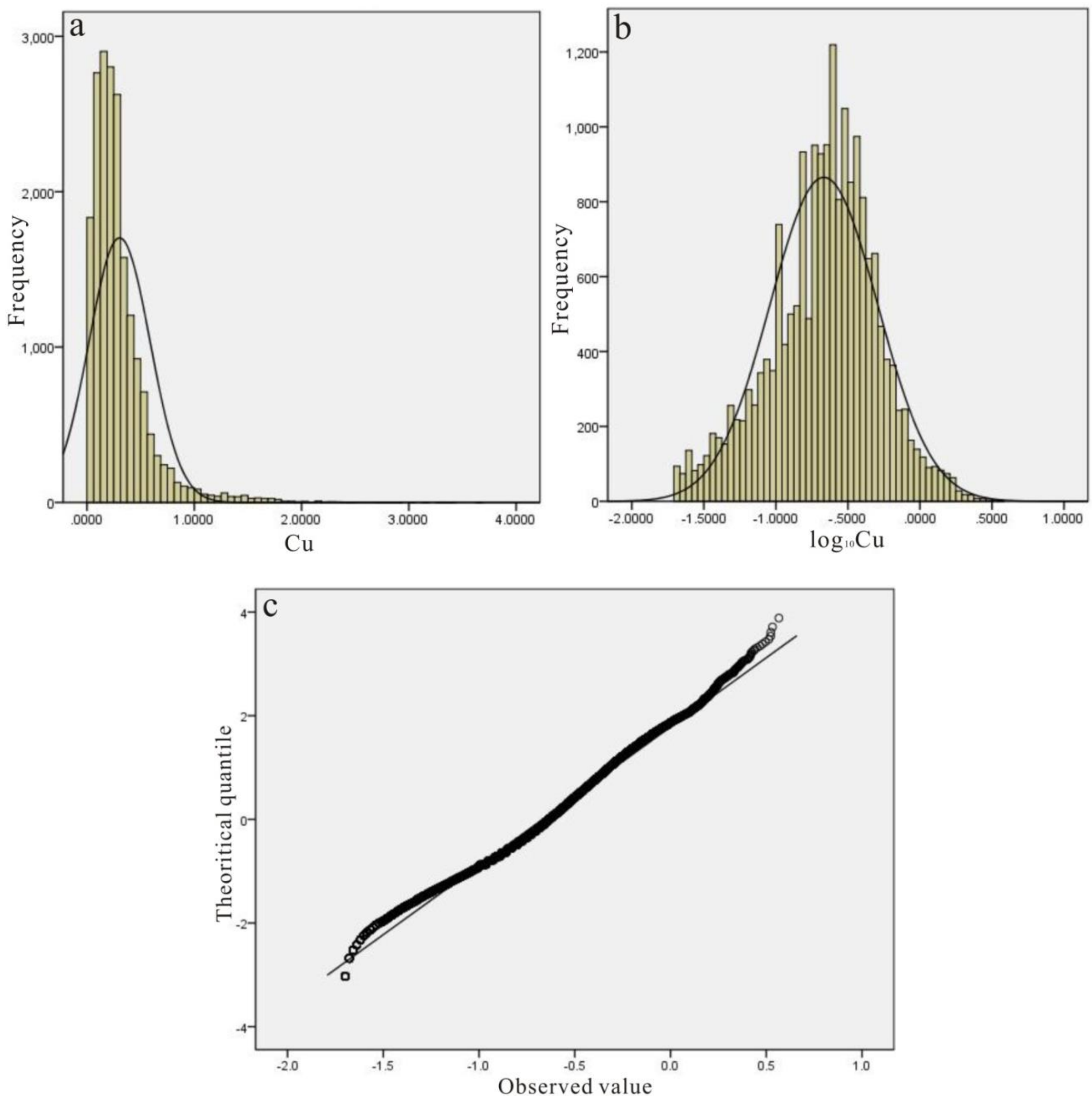
a
Frequency
3,000
2,000
1,000
0
.0000
1.0000
2.0000
3.0000
4.0000
Cu
b
Frequency
1,200
1,000
800
600
400
200
0
-2.0000
-1.5000
-1.0000
-.5000
.0000
.5000
1.0000
log10Cu
c
Theoritical quantile
4
2
0
-2
-4
-2.0
-1.5
-1.0
-0.5
0.0
0.5
1.0
Observed value

Fig. 5.

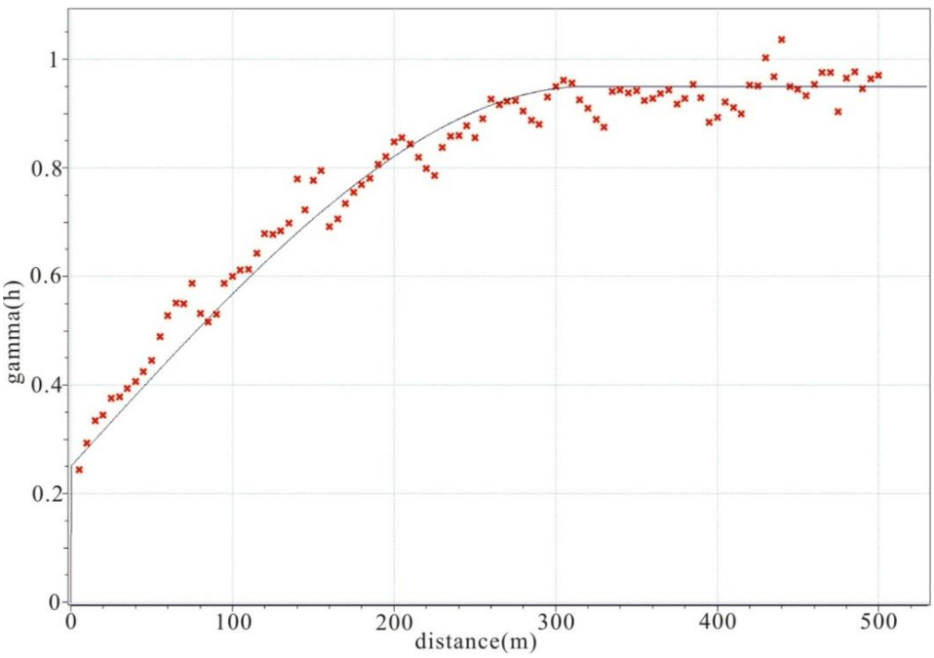
gamma(h)
distance(m)
0
0.2
0.4
0.6
0.8
1
0
100
200
300
400
500

Fig. 6.

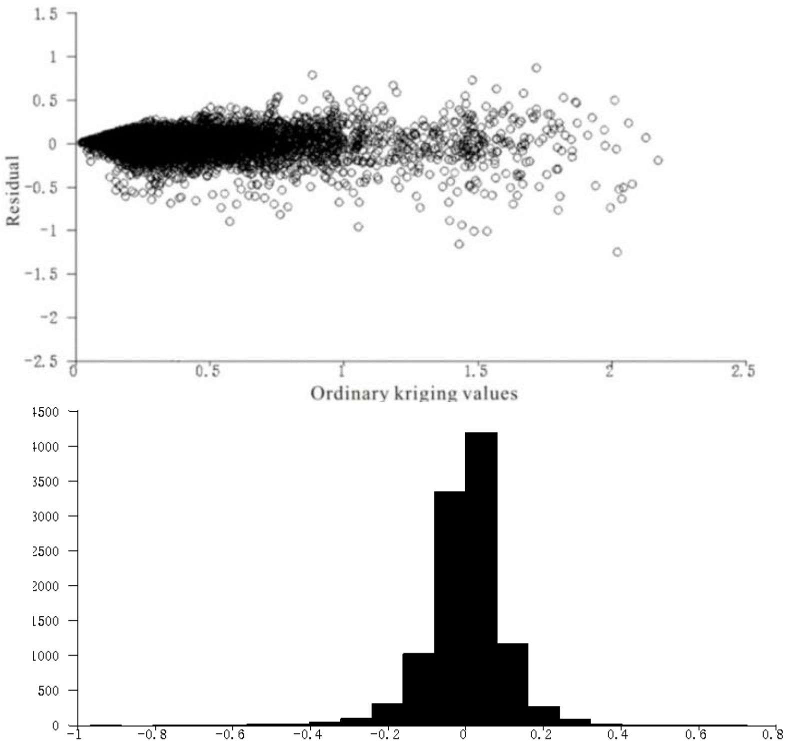
Residual
Ordinary kriging values
1.5
1
0.5
0
-0.5
-1
-1.5
-2
-2.5
0
0.5
1
1.5
2
2.5
4000
3500
3000
2500
2000
1500
1000
500
0
-1
-0.8
-0.6
-0.4
-0.2
0
0.2
0.4
0.6
0.8

Fig. 7.

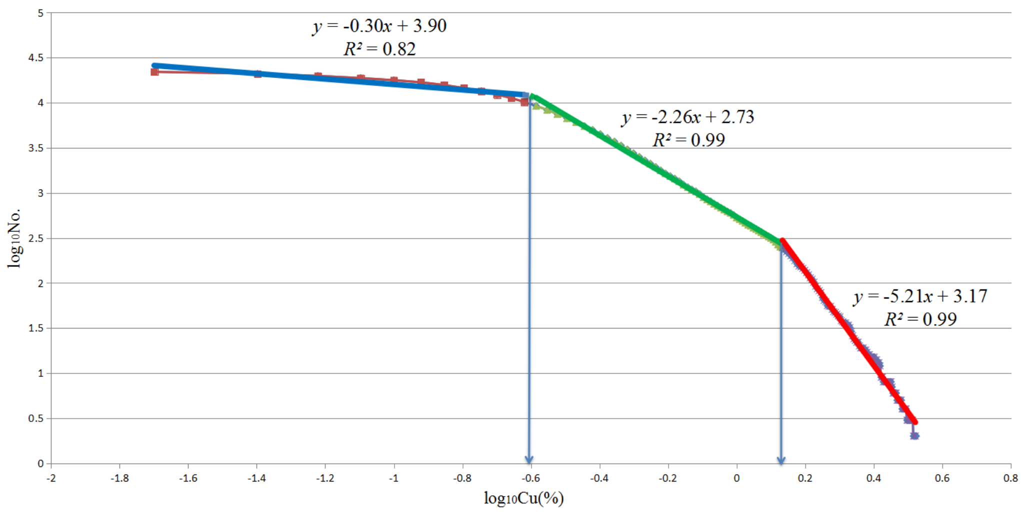
y = -0.30x + 3.90
R² = 0.82
y = -2.26x + 2.73
R² = 0.99
y = -5.21x + 3.17
R² = 0.99
log10No.
log10Cu(%)
0
0.5
1
1.5
2
2.5
3
3.5
4
4.5
5
-2
-1.8
-1.6
-1.4
-1.2
-1
-0.8
-0.6
-0.4
-0.2
0
0.2
0.4
0.6
0.8

Fig. 8.

(a)

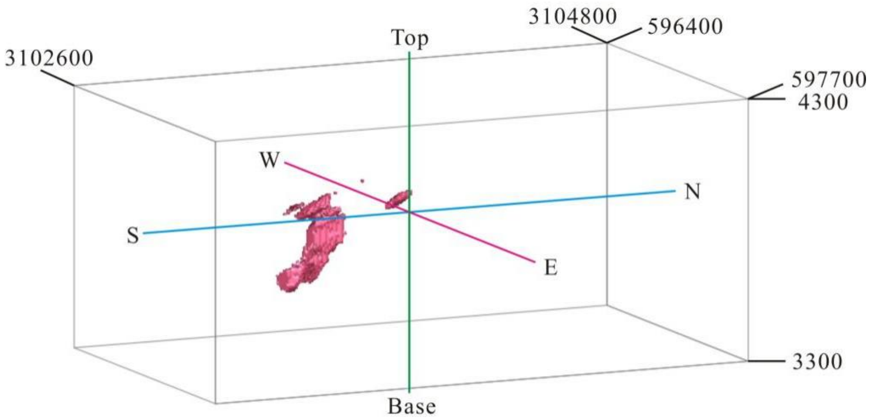
3102600
Top
3104800
596400
597700
4300
W
N
S
E
3300
Base

(b)

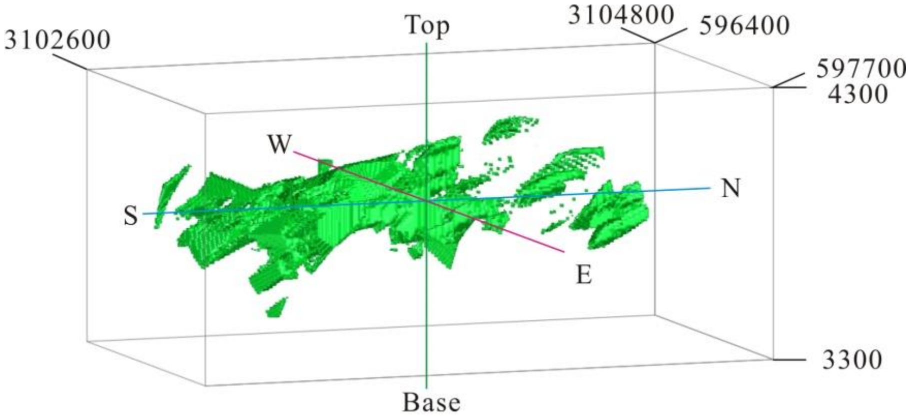
3102600
Top
3104800
596400
597700
4300
W
N
S
E
3300
Base

(c)

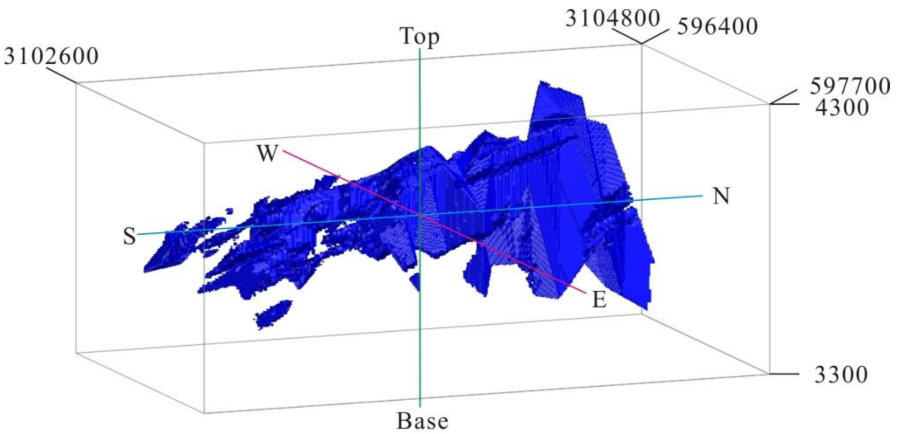
3102600
Top
3104800
596400
597700
4300
W
N
S
E
3300
Base

Fig. 9

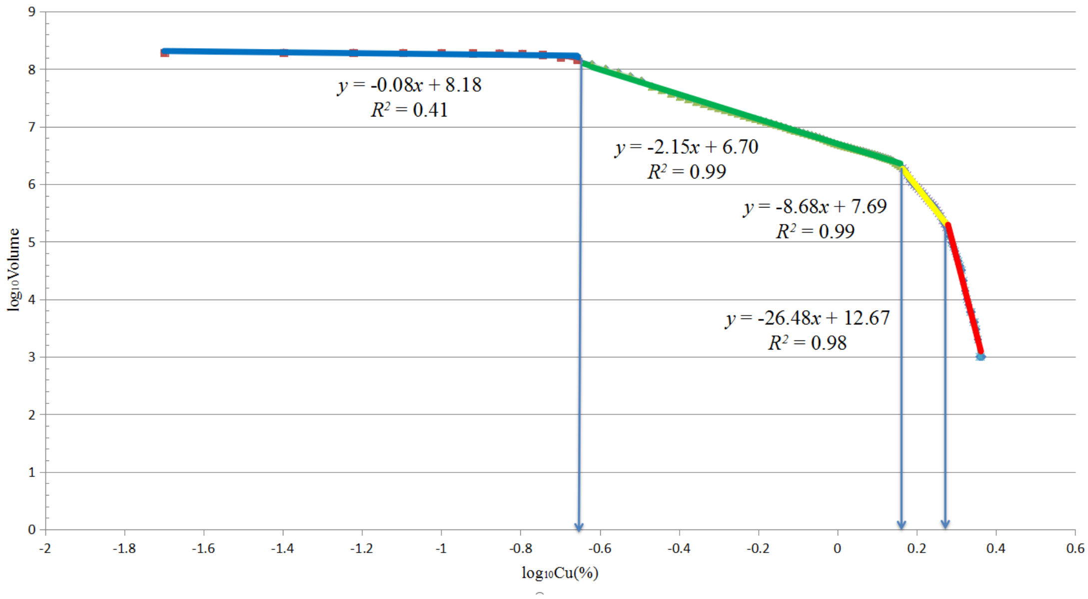

y = -0.08x + 8.18
R² = 0.41
y = -2.15x + 6.70
R² = 0.99
y = -8.68x + 7.69
R² = 0.99
y = -26.48x + 12.67
R² = 0.98
log10Volume
log10Cu(%)
9
8
7
6
5
4
3
2
1
0
-2
-1.8
-1.6
-1.4
-1.2
-1
-0.8
-0.6
-0.4
-0.2
0
0.2
0.4
0.6

Fig. 10.

(a)

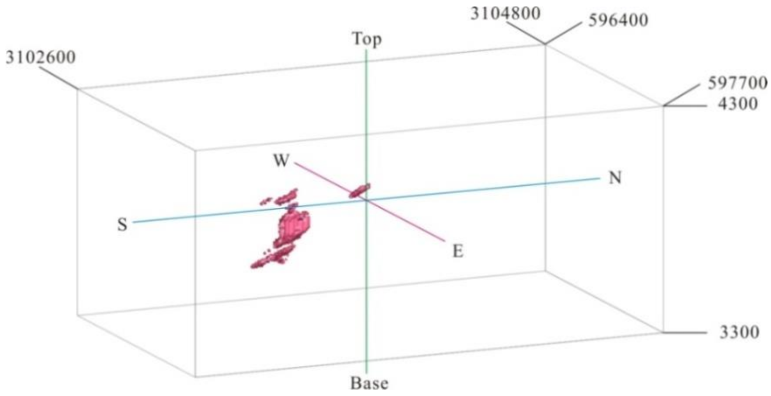

3104800
596400
3102600
Top
597700
4300
W
N
S
E
3300
Base

(b)

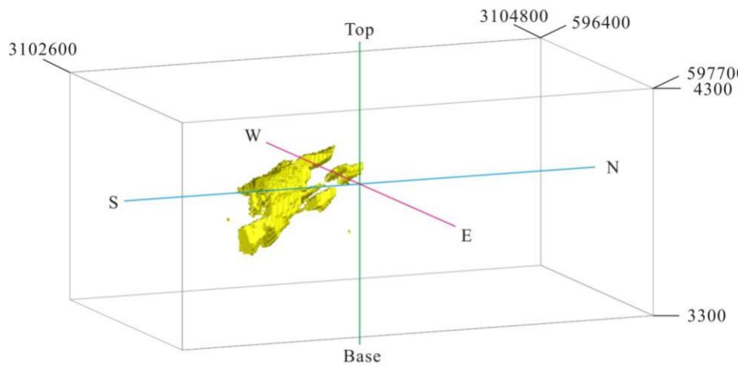

3104800
596400
Top
3102600
597700
4300
W
N
S
E
3300
Base

(c)

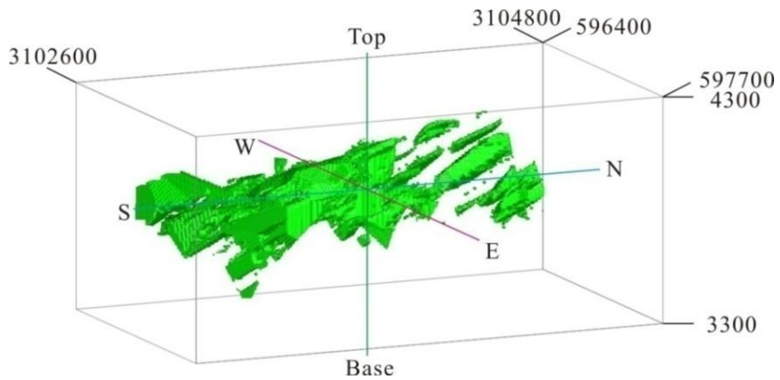

3104800
596400
Top
3102600
597700
4300
W
N
S
E
3300
Base

(d)

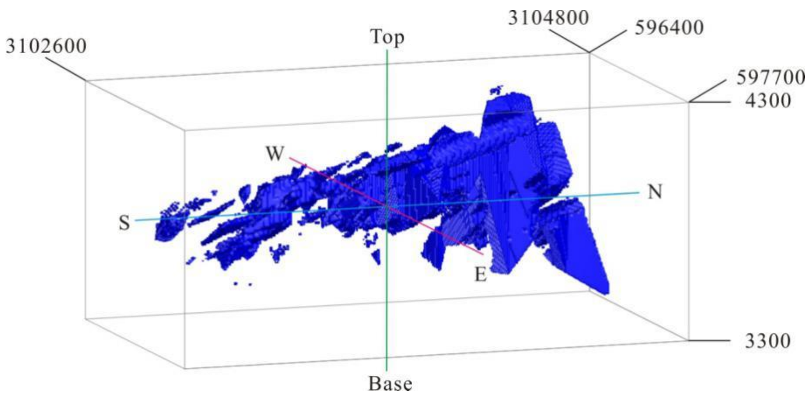

3104800
596400
3102600
Top
597700
4300
W
N
S
E
3300
Base

Fig. 11.

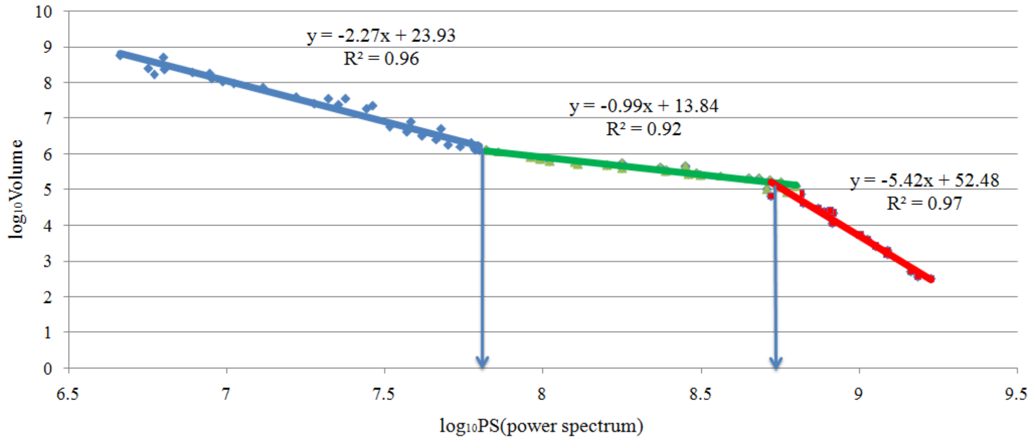

Fig. 12.

(a)

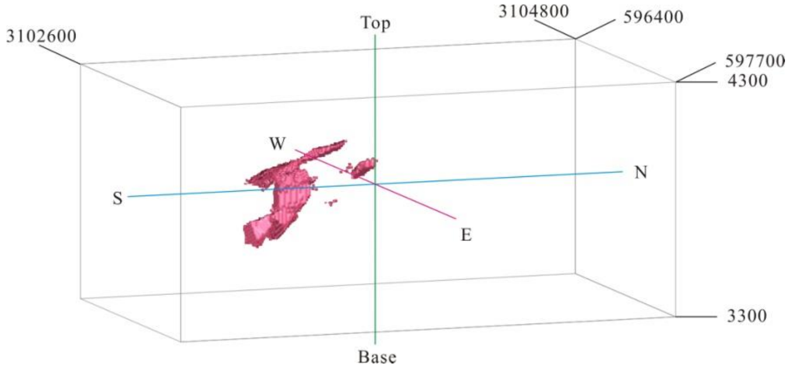

(b)

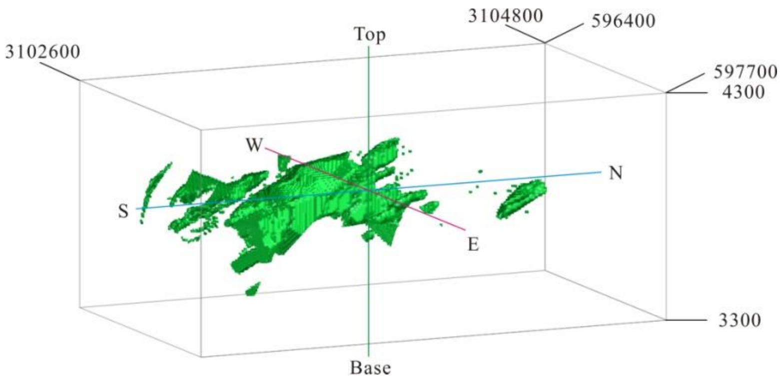

(c)

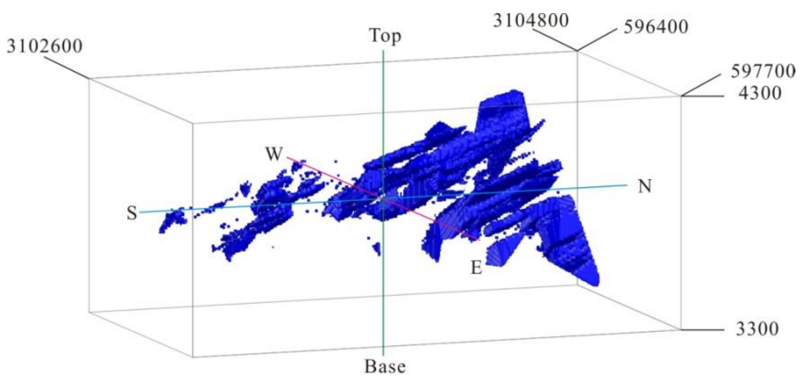

Fig. 13.

(a)

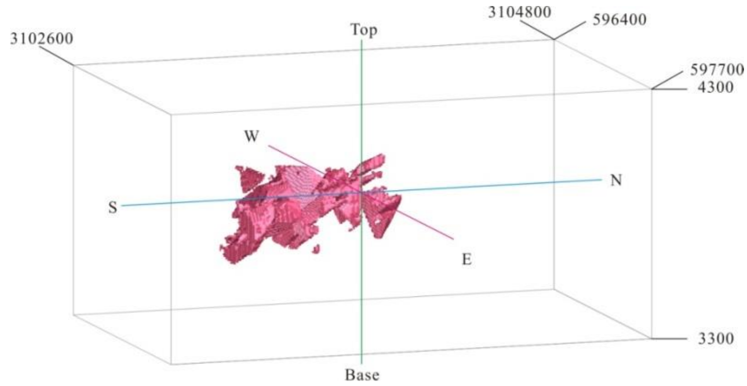

3102600
Top
3104800
596400
597700
4300
W
S
N
E
3300
Base

(b)

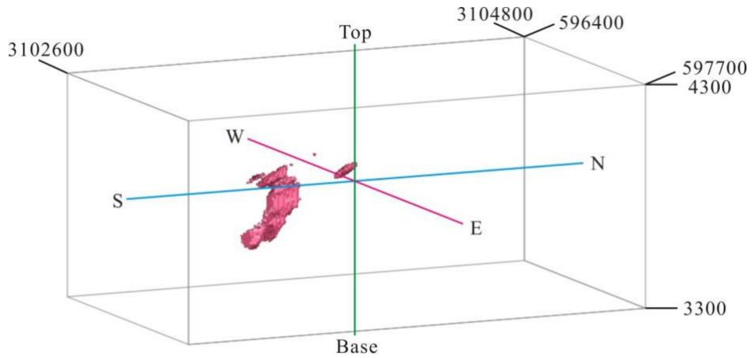

3102600
Top
3104800
596400
597700
4300
W
S
N
E
3300
Base

(c)

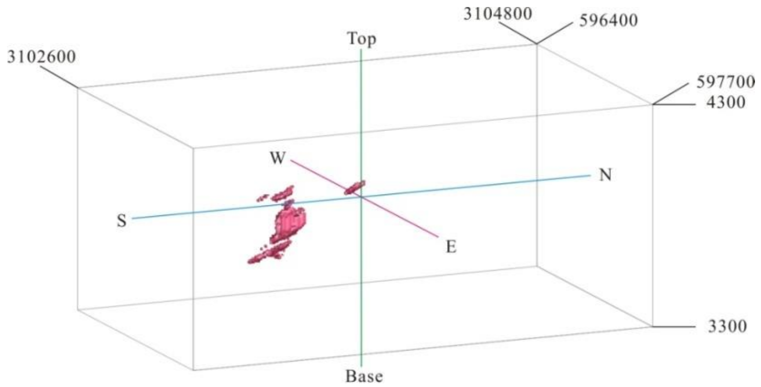

3102600
Top
3104800
596400
597700
4300
W
S
N
E
3300
Base

(d)

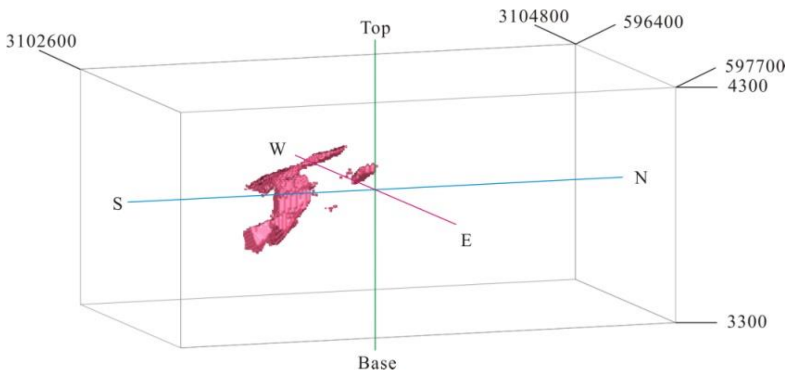

3102600
Top
3104800
596400
597700
4300
W
S
N
E
3300
Base

Fig. 14.

(a)

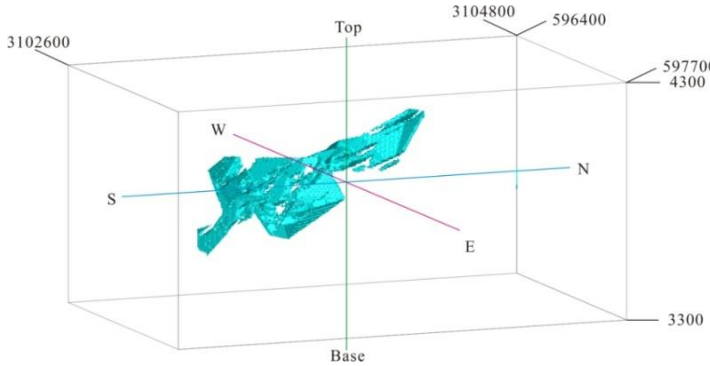

3102600
Top
3104800
596400
597700
4300
W
N
S
E
3300
Base

(b)

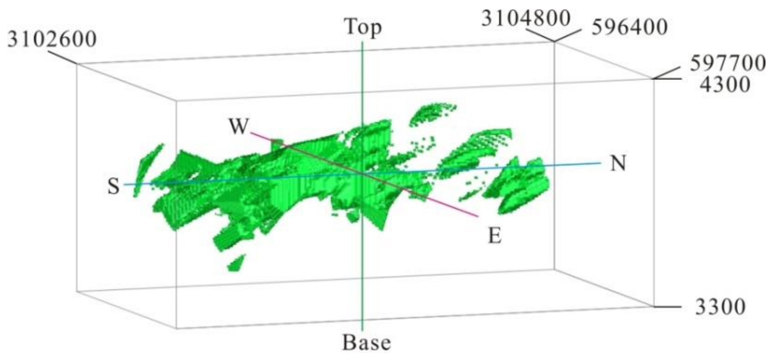

3102600
Top
3104800
596400
597700
4300
W
N
S
E
3300
Base

(c)

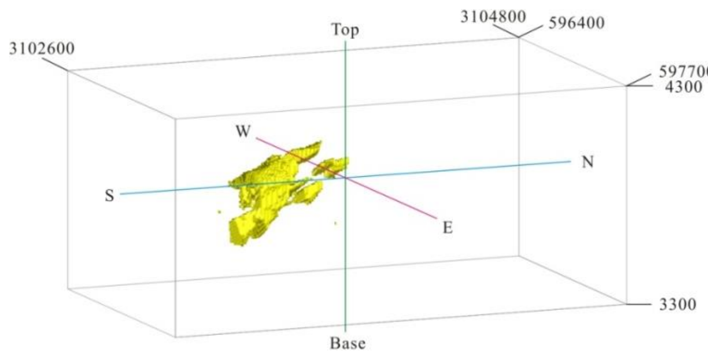

3102600
Top
3104800
596400
597700
4300
W
N
S
E
3300
Base

(d)

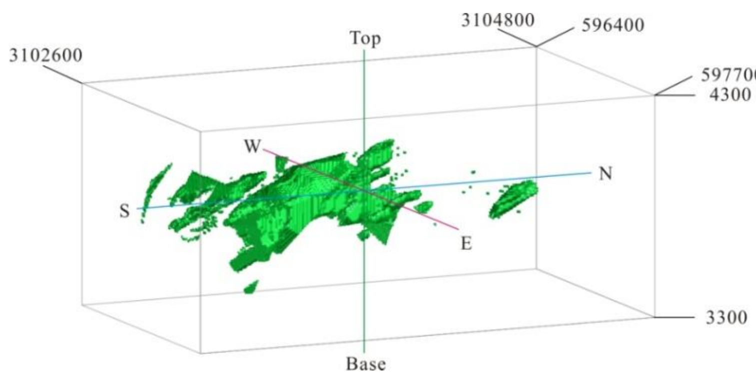

3102600
Top
3104800
596400
597700
4300
W
N
S
E
3300
Base

Fig. 15.

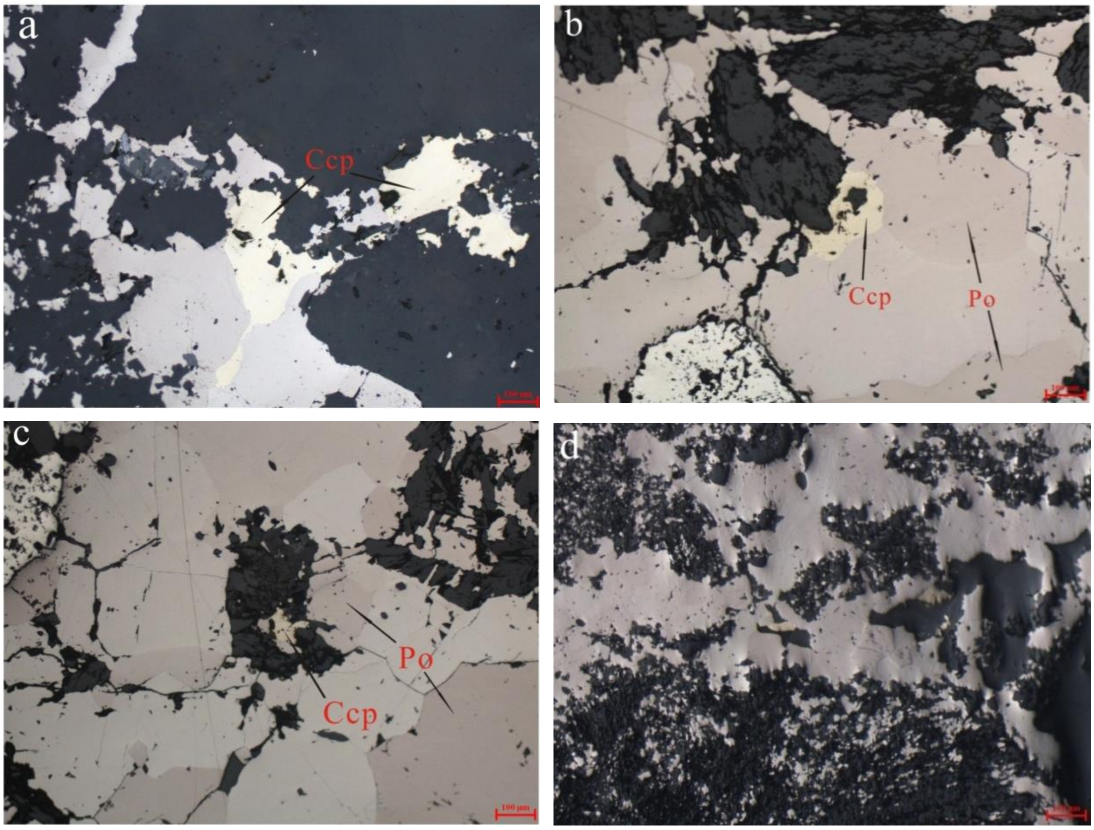

Fig. 16.

Table 1

Variables	Residual
Mean	0.000
Variance	0.016
Standard Deviation	0.127

Table 2

Mineralized zones	Thresholds (Cu%)	Range (Cu%)
Barren host rock and weakly mineralized		<0.28
Moderately mineralized	0.28	0.28-1.45
Highly mineralized	1.45	>1.45

Table 3

Mineralized zones	Thresholds (Cu%)	Range (Cu%)
Barren host rock		<0.25
Weakly mineralized	0.25	0.25–1.48
Moderately mineralized	1.48	1.48–1.88
Highly mineralized	1.88	>1.88

Table 4

Mineralized zones	PS threshold	Range of PS	Range (Cu%)
leached zone and barren host rock		<7.81	<0.23
hypogene zones	7.81	7.81-8.70	0.23-1.33
supergene enrichment zones	8.70	>8.70	>1.33

Table 5

		Geological model	
		Inside zone	Outside zone
Fractal model	Inside zone	True positive (A)	False positive (B)
	Outside zone	False negative (C)	True negative (D)
		TypeIerror=C/(A+C)	TypeIIerror=B/(B+D)
		Overallaccuracy=(A+D)/(A+B+C+D)	

Table 6

		Potassic alteration of geological model	
		Inside zones	Outside zones
C–V fractal model of highly mineralized zones	Inside zones Outside zones	A 2850 C 77927 T1E 0.96 OA	B 1360 D 76913 T2E 0.02 0.50
N–S fractal model of highly mineralized zones	Inside zones Outside zones	A 3092 C 75025 T1E 0.96 OA	B 1570 D 75473 T2E 0.02 0.51
S–V fractal model of supergene enrichment zones	Inside zones Outside zones	A 4431 C 72985 T1E 0.94 OA	B 2318 D 75726 T2E 0.03 0.52

Table 7

		Phyllic alteration of geological model	
		Inside zones	Outside zones
C–V fractal model of moderately and weakly mineralized zones	Inside zones Outside zones	A 36518 C 25461 T1E 0.41 OA	B 48027 D 69155 T2E 0.40 0.59
N–S fractal model of moderately mineralized zones	Inside zones Outside zones	A 35555 C 23955 T1E 0.40 OA	B 46943 D 48223 T2E 0.49 0.54
S–V fractal model of the hypogene zones	Inside zones Outside zones	A 40080 C 26899 T1E 0.40 OA	B 44943 D 54239 T2E 0.45 0.56

Table 8

Sample no.	Mineralized zones obtained by fractal models	Cu (%)
PL-B74	Weakly mineralized zones	0.41
PL-B62	Moderately mineralized zones	1.32
PL-B82	Highly mineralized zones	1.80